Nano/Microstructural Effect of Hydroxyapatite Nanocrystals on Hepatocyte Cell Aggregation and Adhesion

Motohiro Tagaya,* Tomohiko Yamazaki, Daiji Tsuya, Yoshimasa Sugimoto, Nobutaka Hanagata, Toshiyuki Ikoma

Hepatocyte cell aggregation and adhesion to HAp nanocrystals covered with SU-8 polymer micropatterns by nano/microfabrication techniques is demonstrated. The surface roughness and wettability of the HAp nanocrystals are significantly different from those of the SU-8 polymer. QCM-D and microscopic observation clearly reveal that the cells realize the surface properties to form aggregation and preferentially adhere to the HAp nanocrystals at 2 h after seeding, indicating the importance of the microstructures as well as the interfacial phenomena at a nanometer scale.

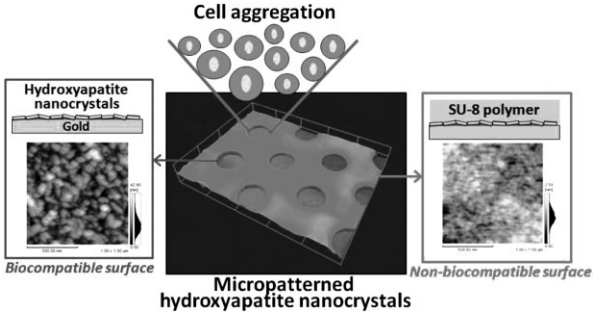

Introduction

Cells in tissues exist in a three-dimensional (3D) environment where cellular shapes and cell–cell interactions play important roles in cell behaviors such as proliferation, migration, differentiation, and survival. In contrast, cells in most tissue cultures exist in a two-dimensional (2D) environment[1] that lacks such morphological and architectural characteristics. Fabrication of in vivo-like microenvironments may lead to advances in diverse fields.[2–4]

Dr. M. Tagaya, Prof. T. Ikoma
Department of Metallurgy and Ceramics Science, Graduate School of Science & Engineering, Tokyo Institute of Technology, O-okayama 2-12-1, Meguro-ku, Tokyo 152-8550, Japan
E-mail: tagaya.m.aa@m.titech.ac.jp
Dr. M. Tagaya, Dr. T. Yamazaki, Dr. N. Hanagata, Prof. T. Ikoma
Biomaterials Center, National Institute for Materials Science, Sengen 1-2-1, Tsukuba, Ibaraki 305-0047, Japan
Dr. D. Tsuya, Dr. Y. Sugimoto
3-D Nano-Integration Foundry, National Institute for Materials Science, Sengen 1-2-1, Tsukuba, Ibaraki 305-0047, Japan

One means of developing such a microenvironment is to form 3D cellular aggregation (spheroids). Particularly attractive techniques for tissue engineering would be the capability to use micropatterning for the cell aggregation. To this end, geometric features have been fabricated with non-cellular adhesive polymers such as poly(ethylene glycol) (PEG)[5–7] in which the micropatterned surfaces form regions of low shear stress for cell immobilization and subsequent spheroid formation. In addition, micropatterned co-cultures of hepatocyte spheroids and fibroblast monolayers have been fabricated for precisely controlling cell–cell interactions.[8]

To date, however, adhesion behavior involving aggregation in a biological environment has not been reported in detail. Both hepatocyte cell aggregation on non-biocompatible surfaces and their subsequent adhesion on biocompatible surfaces are attractive areas. On the other hand, cell adhesion depends on nanometer-scale surface properties such as topography, wettability, and charge and on protein adsorption on materials.[9–13] In addition, the surface distance between gold (Au) nanoparticles modified with arginine-glycine-asparagine (RGD) peptides, in which the cells are well adhered and well spread, is reportedly less

DOI: 10.1002/mabi.201100182

than 58 nm, indicating the importance of controlling the interfaces at a nanometer scale.[14] Therefore, the design of the interfacial phenomena on biocompatible materials at a nanometer and micrometer scale is of great importance.

In this study, using quartz crystal microbalance with dissipation (QCM-D) and light microscopy, we investigated hepatocyte cell aggregation and adhesion on the micropatterns (formed using SU-8: an epoxy polymer photoresist) of hydroxyapatite [$Ca_{10}(PO_4)_6(OH)_2$; HAp] nanocrystals. HAp is a biocompatible ceramic[15] that is widely used for applications such as collagen-based bone filling[16–19] and drug delivery.[20–23] We have conducted studies on the interfacial phenomena using the HAp nanocrystal thin film fabricated by electrophoretic deposition (EPD), including investigation of real-time protein adsorption on the surfaces and that of interfacial phenomena between the HAp and cells, as determined by QCM-D.[25–32] On the other hand, the epoxy polymer is commonly used for photoresists in semiconductor manufacturing and can be used to easily form micropatterns. The negative photoresist SU-8 is not biocompatible and has a high contrast and optical transparency above 360 nm, which are suitable for imaging near vertical sidewalls in electronic and biological applications.[8,33,34] Aggregation of the cells and their subsequent adhesion in the presence of both biocompatible HAp and non-biocompatible SU-8 and these complex effects have not been reported on the related interfacial phenomena. Thus, the micropattern fabrication of surfaces with properties that are biocompatible or non-biocompatible as well as the interfacial design was investigated in order to control the aggregation and adhesion of the cells.

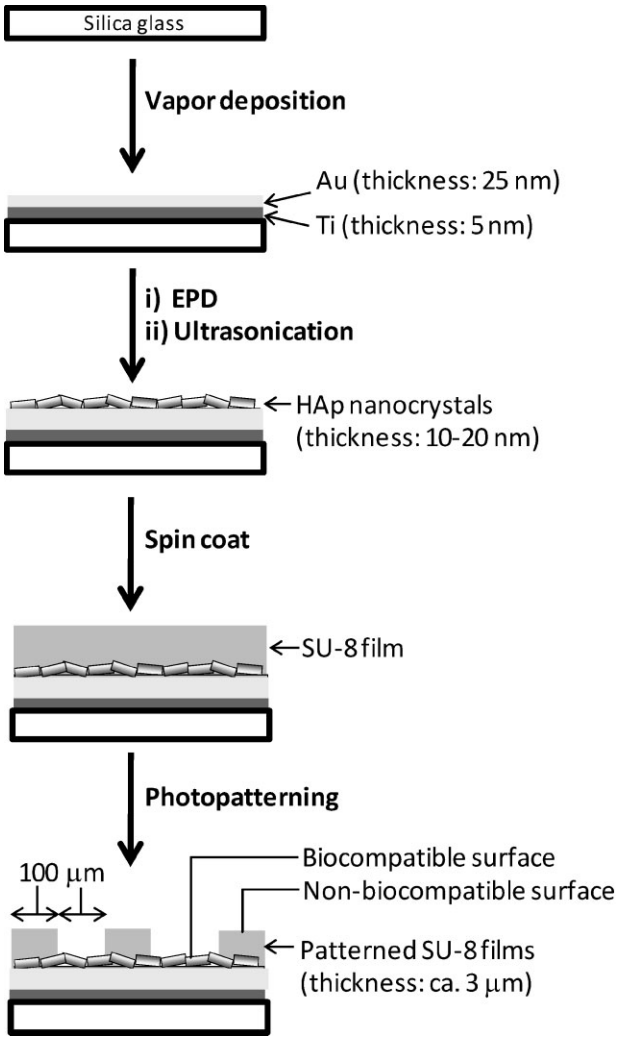

Scheme 1. Schematic illustration of the micropatterning process for the SU-8/HAp nanocrystals/Au/Ti/silica substrate.

Experimental Section

Materials

The following reagents and materials were used: ethanol (99.5 vol%, Wako Co., Ltd.), *t*-butyl alcohol (99 vol%, Wako Co., Ltd.), fetal bovine serum (FBS; model number 12603C, JRH Biosciences Co., Ltd.), Dulbecco's minimum essential medium (DMEM; No. D5796, Aldrich-Sigma Co., Ltd.) as a buffer for protein adsorption, phosphate-buffered saline (PBS; Dulbecco Co., Ltd.), isopropyl alcohol (IPA; special grade, Wako Co., Ltd.), 0.05 wt% trypsin in 0.053 M ethylenediaminetetraacetic acid (EDTA; No. 204-16935, Wako Co., Ltd.), liquid SU-8 and developer solution (SU-8 3010, KMMC Co., Ltd.), formaldehyde (37 vol%, Wako Co., Ltd.), and hepatocytes from the human liver carcinoma cell line (RCB1648, Riken BioResource Center). The following items were used: a Au sensor for use in the QCM-D experiments (QSX-301, Q-Sense Inc.), 35 mm culture dishes (No. 3000-035, Iwaki Co., Ltd.), slide glasses (No. S1112, Matsunami Co., Ltd.), and plastic cell culture flasks (area 75 cm^2, BD Bioscience, Co., Ltd.).

Formation of HAp Nanocrystal Nanolayer

Scheme 1 shows a schematic illustration of the micropatterning process. A slide silica glass was cut to an area of 2×2 cm^2, treated in an ultrasonic bath of ultrapure water (100 mL) for 10 min, dried under N_2 gas flow, and irradiated with UV light ($\lambda = 254$ and 185 nm; UV/Ozone, Bioforce Nanoscience Co., Ltd.) for 10 min. Ti and Au films were deposited on the substrate by radio frequency magnetron sputter deposition (Jsputtter, Alvac Co., Ltd.) under the following sputtering conditions: generating power at 300 W, distance between the cathode and substrate at 12 cm, Ar flow rate at 20 sccm, pressure at 0.01 Pa, and deposition times of 450 s for Ti (thickness 5 nm) and 180 s for Au (thickness 25 nm). The Au sensor and Au/Ti substrate were cleaned by immersion in a 5:1:1 mixture of ultrapure water, H_2O_2, and NH_3 at 70 °C for 10 min, dried under N_2 gas flow, and treated with UV light in air for 10 min.

HAp nanocrystals were deposited by EPD on the Au sensor and Au/Ti substrate surface and as follows, as reported previously.[25,26] The HAp nanocrystals were synthesized at room temperature by a wet chemical method.[24] Dilute H_3PO_4 solution was added to a

$Ca(OH)_2$ suspension until the mixture reached pH = 8.0. The HAp suspension was centrifuged (2 000 *g*, 15 min), washed three times in ethanol, and dispersed ultrasonically in ethanol at 1 wt%. The Au sensor surfaces were used as electrodes and a direct current voltage of 100 $V \cdot cm^{-1}$ was applied for 1 min. Surplus nanocrystals were removed by ultrasonic treatment (28 kHz, 100 W, 1 min) in ethanol.

Photopatterning

The HAp nanocrystal substrate was spin-coated (Opticoat MS-A-150, Mikasa Co., Ltd.) (5 000 rpm, 60 s) with 2.5 mL of liquid SU-8 and then heated at 100 °C for 10 min. The film was photo-patterned on the coating by semiconductor laser irradiation (DL-1000, Nano-system Solutions Co., Ltd.) ($\lambda = 405$ nm, energy 300 $mW \cdot cm^{-2}$, irradiation spot size 100 μm, and interval step size 100 μm). The irradiated film was baked at 100 °C for 10 min, immersed in the SU-8 developer for 5 min, immersed in IPA for 30 s, dried under N_2 gas flow, and baked at 200 °C for 30 min. The micropatterned surfaces were treated with an O_2 plasma system (PB-600, Yamato Science Co., Ltd.) in a quartz chamber (atmosphere O_2, pressure 133 Pa, plasma power 150 W, and treatment time 180 s).

Cell Culture

Hepatocyte cells were cultured in a cell culture flask containing 15 mL of FBS dispersed in DMEM at 10 vol% (10% FBS/DMEM). The cells were incubated at 37 °C in a humidified atmosphere of 5% CO_2, subcultured every 7 d with 1 mL of trypsin/EDTA, washed with 15 mL of PBS, treated with 1 mL of trypsin/EDTA for 5 min at 37 °C, dispersed in 15 mL of PBS, and subjected to two cycles of centrifugation (2000 rpm, 2 min) and dispersion in 15 mL of 10% FBS/DMEM. The number of cells in the suspension was counted and adjusted to a density of 2.5×10^4 cells mL^{-1} for QCM-D measurements.

Protein Adsorption and Cell Adhesion

QCM-D (D300, Q-Sense AB) measurements were performed at 37.0 ± 0.05 °C by real-time monitoring of the changes in resonance frequency shift (Δf) and dissipation shift (ΔD) of the sensor (oscillation at 15 MHz). The measured Δf was divided by the harmonic overtone ($n = 3$) as a fundamental frequency of 5 MHz. DMEM was introduced into the sample chamber for 30–60 min to stabilize the baseline, followed by the introduction of 0.5 mL of 10% FBS/DMEM, and then baseline measurements were taken for 60 min. Subsequently, FBS adlayers on the sensor were seeded with 0.5 mL of a hepatocyte cell suspension in FBS/DMEM (seeding density 2.5×10^3 cells $\cdot cm^{-2}$), cultured in air for 2 h, and rinsed with 0.5 mL of DMEM. Cells cultured on the sensors were removed from the sample chamber, washed two times with 1 mL of PBS, fixed with 3.7 vol% formaldehyde in PBS at room temperature for 10 min, and again washed two times with 1 mL of PBS. The viscoelastic property of the FBS adlayers was evaluated by measurement of the saturated $\Delta D/\Delta f$ value ($\Delta D_{sat}/\Delta f_{sat}$) from $\Delta D/\Delta f$ plots, as described in our previous report.[25] The weight change by protein adsorption was calculated from the Sauerbrey equation,[35]

$$\Delta m = -C \times \Delta f \quad (1)$$

where C is a constant equal to 17.7 ng $\cdot Hz^{-1} \cdot cm^{-2}$.

Cell Aggregation and Adhesion on the Micropattern

The hepatocyte cells were cultured on the micropattern in a humidified atmosphere of 5% CO_2 as follows. First, 3 mL of DMEM was added on the micropattern surface, cultured statically for 30–60 min, and then removed. Then, 3 mL of 10% FBS/DMEM was added on the surface, cultured statically for 60 min, and then removed. Finally, a solution of dispersed hepatocyte cells was added on the surface at a seeding density of 2.5×10^3 cells $\cdot cm^{-2}$ and cultured statically for 2 h.

Characterization

Crystallinity of the HAp nanocrystals was characterized by X-ray diffraction (XRD). The nanocrystal surfaces were analyzed by atomic force microscopy (AFM; SPM-9500, Shimazu Inc.) using a silicon probe mounted on a cantilever (OMCL-AC160TS, Olympus Inc.) for the dynamic mode. Surface roughness (R_{rms}) was calculated by root mean squares (RMS) in the *Z*-range images. The morphology of the nano/micropatterns and cells cultured on the surfaces was observed by confocal laser scanning microscopy (CLSM; OLS-3000, Olympus Inc.). In the 2D images, the numbers of adherent cells on the sensors were counted in 20 different 1 mm^2 areas, and the spreading areas for the cells were measured for 50 cells. 3D images of the nano/micropatterns and cells were acquired in 20–50 horizontal sections from top to bottom in the vertical direction. Wettability of the sensor surfaces was analyzed in air by a sessile drop method using distilled water with a contact angle meter (CA-W200, Kyowa Interface Science Inc.) (droplet volume 1.5 μL and area attached on the surfaces 1.6 mm^2). Cell aggregation was observed by optical microscopy (IX81, Olympus Co., Ltd.) at 37 °C in a humidified atmosphere of 5% CO_2.

Results and Discussion

Preferential Cell Adhesion to HAp Nanocrystals

The XRD pattern of the synthesized nanocrystals indicated the absence of other phases, and the large peak width indicated that the crystalline domains were small in size, consistent with our previous reports.[24,25,29] The weight change of the HAp nanocrystals on the Au sensor in air was 4.0 ± 0.2 μg $\cdot cm^{-2}$, as determined by QCM-D, and the thickness was calculated to be 12.9 ± 0.5 nm (assuming the HAp density to be 3.14 g $\cdot cm^{-3}$).[26,28] The HAp nanocrystals deposited on the Au sensor had the R_{rms} value of 4.2 ± 0.8 nm. Thus, the QCM-D sensor with the HAp nanocrystals was successfully fabricated by the EPD method.

Preferential protein adsorption and subsequent cell adhesion to the HAp nanocrystals have previously been determined by QCM-D and reported.[30,31,36,37] FBS protein adsorption from DMEM solvent reached an equilibrium state for 60 min, as determined from Δf and ΔD curves. At 60 min, adsorption amount was 0.73 ± 0.06 μg $\cdot cm^{-2}$ and the $\Delta D_{sat}/\Delta f_{sat}$ value was $-3.2 \pm 1.8 \times 10^{-8}$ Hz^{-1}.[28] Thus,

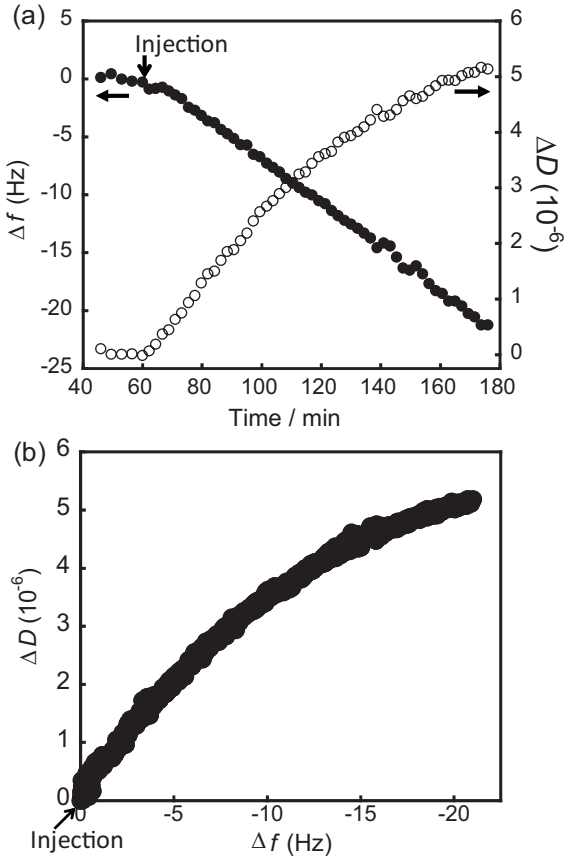

Figure 1. Plots of hepatocyte cell adhesion on a HAp nanocrystal surface measured by QCM-D: (a) Δf (solid circles) and ΔD (open circles) curves; (b) $\Delta D/\Delta f$ plot.

the carbonate ion adsorption from DMEM promoted less FBS adsorption and increased degradation of the viscoelastic property of the FBS adlayer as compared to the adsorption from PBS.

Figure 1 shows plots of Δf and ΔD changes as a function of time and a ΔD-Δf plot for the hepatocyte cell adhesion on the FBS-modified HAp surface. At 2 h, Δf and ΔD are -20.9 ± 4.2 Hz and $+5.1 \pm 1.2 \times 10^{-6}$, respectively, and the $\Delta D_{sat}/\Delta f_{sat}$ value is $-10.8 \pm 3.1 \times 10^{-8}\,Hz^{-1}$. These results are consistent with those of our previous report.[36] The absolute values of Δf and $\Delta D_{sat}/\Delta f_{sat}$ for the cell adhesion on the HAp nanocrystals were much larger than those on an oxidized polystyrene surface, i.e., at 2 h, the interfacial interactions between the cells and HAp are stronger than those between the cells and the polystyrene. Therefore, hepatocyte cell adhesion clearly depended on surface properties, and the cells preferentially adhered to the biocompatible HAp nanocrystals.

Figure 2 shows 2D and 3D CLSM images and atomic force microscopy (AFM) images of hepatocyte cells adhered to the HAp nanocrystals at 2 h after seeding. From the CLSM images, the cells had a round morphology [Figure 2 (a, b)]. The density and area of adherent cells were determined to be 278 ± 89 cells $\cdot$ cm^{-2} and $379 \pm 127\ \mu m^2 \cdot cell^{-1}$, respectively, which are smaller than for fibroblasts.[37] From the AFM topographic and phase shift images, the cells expanded their pseudopods on the HAp surfaces were observed [Figure 2 (c, d)], although the cellular morphologies seemed to indicate no spreading and cuboidal shapes as compared with those on the other surfaces.[36] The cellular surface had rough fibrous structures ($R_{rms} = 41.3 \pm 5.1$ nm), indicating infection of a cytoskeleton. Therefore, the hepatocyte cells adhered to HAp changed the cytoskeleton and rearranged the extracellular matrix at the interfaces.

Surface Properties of the Micropattern

Figure 3 shows optical microscopy and 3D graphic images of the micropatterned surfaces. Holes of diameter 100 μm were homogeneously formed at intervals of 100 μm through the SU-8 film [Figure 3 (a)]. The film thickness between the SU-8 and HAp nanocrystal surfaces was $2.9 \pm 0.7\ \mu m$, which is lower than the height of the living cells [Figure 3 (b)].

Figure 4 shows AFM topographic images of Au, oxidized HAp nanocrystals, and the SU-8 film. The Au surface had a dense particulate morphology. Table 1 shows that the Au surface has a contact angle for water of $82.4 \pm 2.7^\circ$ and R_{rms} of 1.7 ± 0.3 nm [Figure 4 (a)]. The surface after EPD showed plate-like nanocrystals [Figure 4 (b)] with a contact angle of $48.3 \pm 3.1^\circ$ and R_{rms} of 6.4 ± 0.8 nm (Table 1), which correspond to the surface properties of the HAp sensor mentioned above, indicating deposition of the HA nanocrystals on the Au surface.

The HAp surface promoted cohesive formation of the SU-8 film, indicating preferential adhesion of the HAp nanocrystals to the film. After direct formation of the SU-8 film on Au, the film was easily peeled, indicating weak adhesiveness between hydrophobic Au and SU-8. The SU-8 film on the HAp nanocrystals has a fibrous morphology [Figure 4 (c)], contact angle of $88.6 \pm 2.6^\circ$, and R_{rms} of 0.3 ± 0.1 nm (Table 1), indicating that it is hydrophobic and has a flat surface.

SU-8 contains sulfonium salt, which acts as a photo acid-generating agent. The salt contains both cationic and anionic parts; the anionic part generates acid by photoabsorption, and subsequent photodissociation occurs with hydrogen abstraction from solvents. Thus, hexafluoroantimonic acid ($HSbF_6$) is newly generated on the SU-8 epoxy groups by intramolecular hydrogen transfer coordinates, while simultaneously, the other epoxy groups attack the coordination part to generate oxonium cation. Ring-opening polymerization among the epoxy groups that reacted with the oxonium cation leads to the formation of the

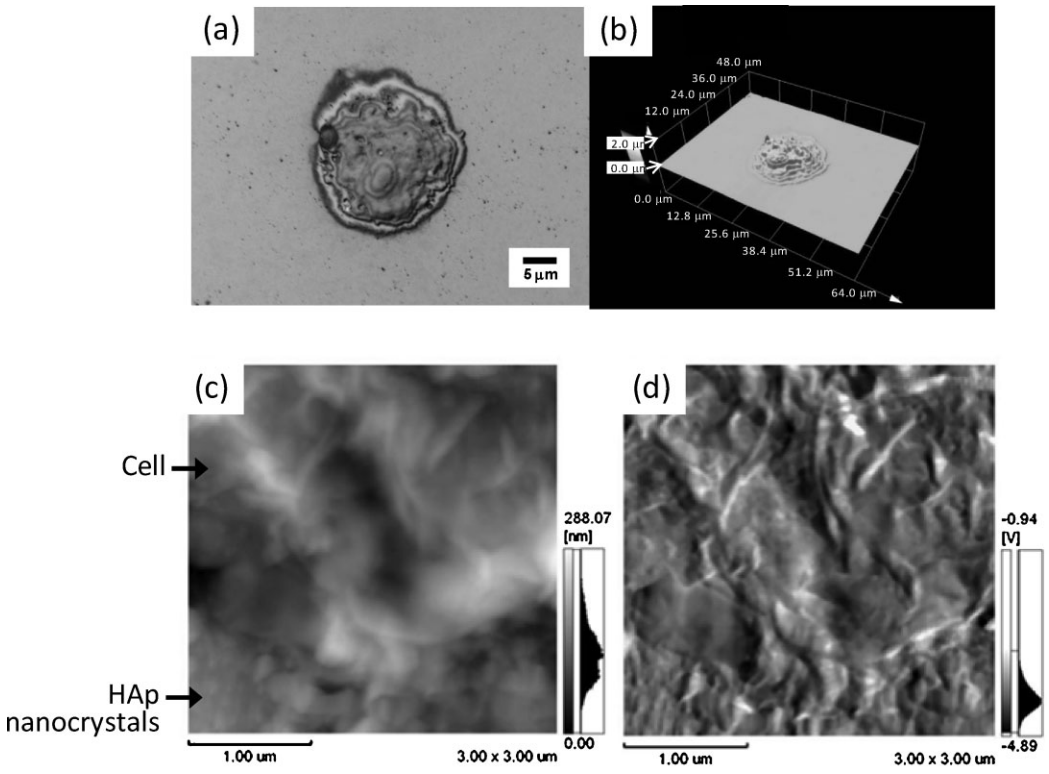

Figure 2. Adhered cell and HAp surfaces: (a) Optical microscopic image of a cell; (b) 3D graphic image of the cell; (c) AFM topographic and (d) phase shift images of the cell and HAp nanocrystal surfaces.

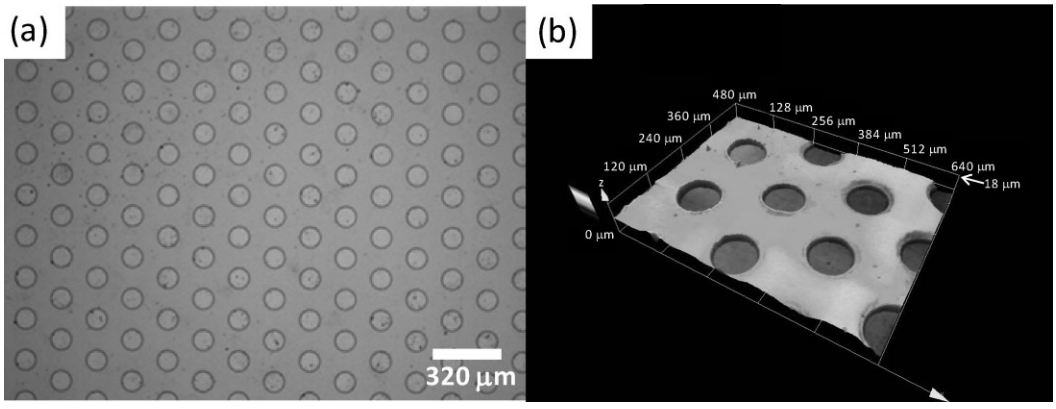

Figure 3. Photopatterned surfaces: (a) Optical microscopic image; (b) 3D graphic image.

polymerized SU-8 film.[38] Thus, the SU-8 film exhibited hydrophobicity due to the polymerized epoxy groups.

With O_2 plasma treatment, the R_{rms} values for HAp and SU-8 remain almost constant, whereas the contact angles change to hydrophilic ($16.2 \pm 2.5^\circ$) for HAp and superhydrophilic ($<5^\circ$) for SU-8 (Table 1). Ablation and subsequent weakening of the superficial region on the polymeric materials is known to occur as a result of corona or plasma treatment.[39,40] Dissociation reaction with collision between electron (e^-) and O_2 occur by treatment, as shown in Equation 2 and 3. A triplet oxygen atom $O(^3P)$ effectively generates a singlet oxygen atom $O(^1D)$, which attacks and etches the substrate surface.[41]

$$e^- + O_2 \rightarrow O(^3P) + O(^1D) + e^- \quad (2)$$

$$e^- + O(^3P) \rightarrow O(^1D) + e^- \quad (3)$$

UV-irradiated HAp nanocrystal surface has been reported by our group,[29] and UV treatment decreased the contact angle slightly to $19 \pm 3^\circ$, which corresponds to

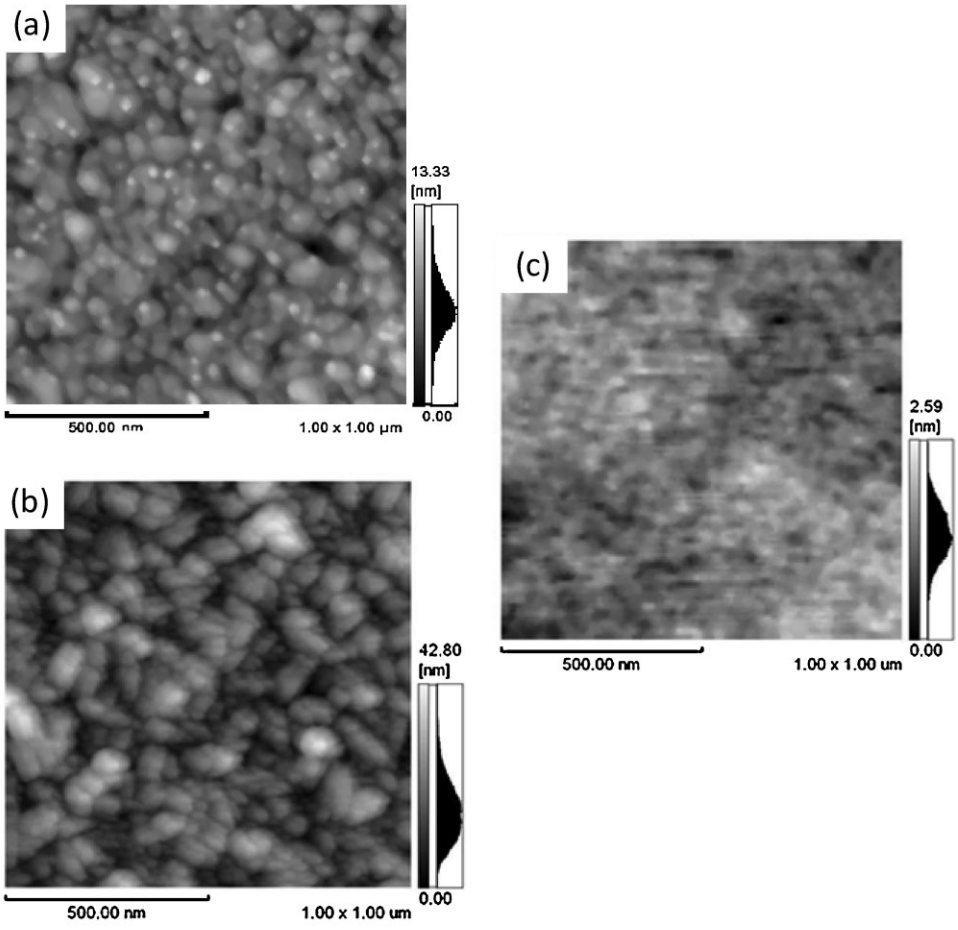

Figure 4. AFM topographical images of the surfaces: (a) Au; (b) HAp nanocrystals; (c) SU-8 film. The area size is 1.0 μm × 1.0 μm.

Table 1. Film thickness, water contact angle, and surface roughness (R_{rms}) of the surfaces.

Surface	Film thickness [nm]	Contact angle [°]	Surface roughness, R_{rms} [nm]
Au	25	82.4 ± 2.7	1.7 ± 0.3
HAp	10–20	48.3 ± 3.1	6.4 ± 0.8
SU-8	2900	88.6 ± 2.6	0.3 ± 0.1
oxidized HAp	–	16.2 ± 2.5	6.2 ± 0.7
oxidized SU-8	–	< 5	0.3 ± 0.2

the present result by the O_2 plasma treatment. Accordingly, the generated $O(^1D)$ would react with the HAp surface to form hydroxyl groups. It also dissociates C–O–C and C–C groups in the SU-8 epoxy group to generate hydrophilic ≡C–OH and –COOH groups.[38] Therefore, a microstructure of hydrophilic HAp nanocrystals surrounded by a superhydrophilic SU-8 wall were successfully fabricated.

Cell Aggregation and Adhesion on the Micropattern

Figure 5 shows microscope images of hepatocyte cell aggregation and adhesion. The cells gathered on the SU-8 surface and subsequently approached the HAp nanocrystals at 0.5 h after seeding [Figure 5(a)], indicating cellular realization of biocompatibility and non-biocompatibility. At 1 h, the aggregated cells were completely on the hole [Figure 5(b)]. At 2 h, the cells adhered to the bottom surface, with only a few cells remaining on the SU-8 surfaces [Figure 5(c)]. The adhesion ratio on the HAp surface was approximately 60%–80% by the observation. It has been reported that proteins tend not to adsorb to superhydrophilic surfaces;[42] therefore, the present results indicate that the superhydrophilic SU-8 surface repels proteins and cells and thereby promotes the formation of aggregation. In contrast, the HAp surface promoted preferential cell adhesion, consistent with our QCM-D results and previous reports.[30,31,36,37] Therefore, the real-time observations indicated that the SU-8 surface repels cell adhesion to form aggregation by cell–cell interactions, and subsequently the

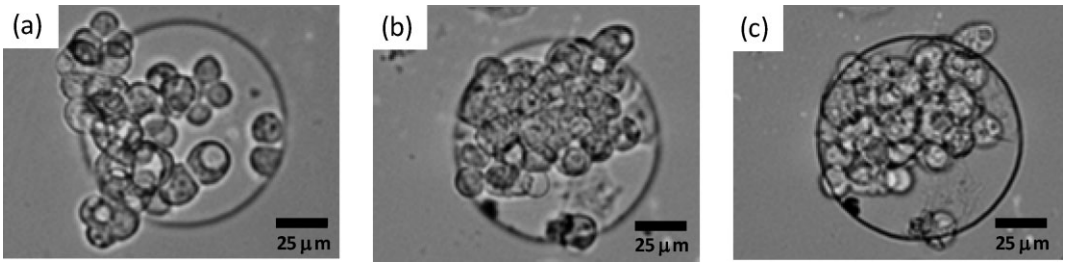

Figure 5. Microscopic images of cells cultured on the micropattern at various times after seeding: (a) 0.5, (b) 1, (c) 2 h.

HAp surface attracts cells and promotes their adhesion and simultaneous aggregation on the surface.

Conclusion

We successfully achieved the aggregation and preferential adhesion of hepatocyte cells to the HAp nanocrystals using a SU-8 polymer micropattern. The preferential adhesion to the HAp nanocrystals was confirmed by the QCM-D technique. The HAp nanocrystals and SU-8 polymer treated by O_2 plasma treatment shows the contact angles for water of $16.2 \pm 2.5^\circ$ and $<5^\circ$, respectively. The cells realized the different surface properties, and promoted cell–cell interactions to form aggregation and subsequently preferential adherence to the HAp nanocrystals. The nano/microfabrication techniques will enable fabrication of spheroid culture systems.

Received: May 20, 2011; Revised: July 4, 2011; Published online: August 25, 2011; DOI: 10.1002/mabi.201100182

Keywords: adhesion; biocompatibility; microstructure; nanoparticles; tissue engineering

[1] A. Abbott, *Nature* **2003**, *424*, 870.
[2] R. Langer, J. P. Vacanti, *Science* **1993**, *260*, 920.
[3] S. Levenberg, R. Langer, *Curr. Top. Dev. Biol.* **2004**, *61*, 113.
[4] A. Khademhosseini, R. Langer, J. Borenstein, J. P. Vacanti, *Proc. Natl. Acad. Sci. USA* **2006**, *103*, 2480.
[5] A. Khademhosseini, J. Yeh, S. Jon, G. Eng, K. Y. Suh, J. A. Burdick, R. Langer, *Lab. Chip* **2004**, *4*, 425.
[6] J. Fukuda, Y. Sakai, K. Nakazawa, *Biomaterials* **2006**, *27*, 1061.
[7] J. Fukuda, K. Nakazawa, *Tissue Eng.* **2005**, *11*, 1254.
[8] J. Fukudaa, A. Khademhosseinib, Y. Yeoa, X. Yanga, J. Yeha, G. Enga, J. Blumlinga, C. F. Wanga, D. S. Kohaned, R. Langera, *Biomaterials* **2006**, *27*, 5259.
[9] A. El-Ghannam, P. Ducheyne, I. M. Shapiro, *J. Orthop. Res.* **1999**, *17*, 340.
[10] M. Rouahi, E. Champion, O. Gallet, A. Jada, K. Anselme, *Colloids Surf. B: Biointerf.* **2006**, *47*, 10.
[11] K. Anselme, *Biomaterials* **2000**, *21*, 667.
[12] B. Kasemo, *Surf. Sci.* **2002**, *500*, 656.
[13] F. Barrere, T. Mahmood, K. Degroot, C. Vanblitterswijk, *Mater. Sci. Eng. R* **2008**, *59*, 38.
[14] M. Arnold, E. A. Cavalcanti-Adam, R. Glass, J. Bluemmel, W. Eck, M. Kantlehner, H. Kessler, J. P. Spatz, *ChemPhysChem.* **2004**, *5*, 383.
[15] M. I. Kay, R. A. Young, A. S. Posner, *Nature* **1964**, *204*, 1050.
[16] M. Kikuchi, S. Itoh, S. Ichinose, K. Shinomiya, J. Tanaka, *Biomaterials* **2001**, *22*, 1705.
[17] L. Letic-Gavrilovic, A. Piattelli, K. Abe, *J. Mater. Sci., Mater. Med.* **2003**, *14*, 95.
[18] S. S. Liao, F. Z. Cui, *Tissue Eng.* **2004**, *10*, 73.
[19] S. Yunoki, T. Ikoma, A. Monkawa, K. Ohta, M. Kikuchi, S. Sotome, K. Shinomiya, J. Tanaka, *Mater. Lett.* **2006**, *60*, 999.
[20] W. Paul, C. P. Sharma, *J. Biomater. Appl.* **2003**, *17*, 253.
[21] H. W. Kim, J. C. Knowles, H. E. Kim, *J. Biomed. Mater. Res., B* **2005**, *74*, 686.
[22] Y. Mizushima, T. Ikoma, J. Tanaka, K. Hoshi, T. Ishihara, Y. Ogawa, A. Ueno, *J. Controlled Release* **2006**, *110*, 260.
[23] T. Ikoma, T. Tonegawa, H. Watanabe, G. P. Chen, J. Tanaka, Y. Mizushima, *J. Nanosci. Nanotech.* **2007**, *7*, 822.
[24] T. Ikoma, A. Yamazaki, S. Nakamura, M. Akao, *J. Solid State Chem.* **1999**, *144*, 272.
[25] A. Monkawa, T. Ikoma, S. Yunoki, T. Yoshioka, J. Tanaka, D. Chakarov, B. Kasemo, *Biomaterials* **2006**, *27*, 5748.
[26] T. Ikoma, M. Tagaya, N. Hanagata, T. Yoshioka, D. Chakarov, B. Kasemo, J. Tanaka, *J. Am. Ceram. Soc.* **2009**, *92*, 1125.
[27] M. Tagaya, T. Ikoma, T. Takemura, M. Okuda, N. Hanagata, T. Yoshioka, D. Chakarov, B. Kasemo, J. Tanaka, *Key Eng. Mater.* **2009**, *396–398*, 47.
[28] M. Tagaya, T. Ikoma, S. Migita, M. Okuda, T. Takemura, N. Hanagata, T. Yoshioka, J. Tanaka, *Mater. Sci. Eng. B* **2010**, *173*, 176.
[29] M. Tagaya, T. Ikoma, D. N. Hanagata, D. Chakarov, B. Kasemo, J. Tanaka, *Sci. Technol. Adv. Mater.* **2010**, *11*, 045002.
[30] M. Tagaya, T. Ikoma, T. Takemura, N. Hanagata, T. Yoshioka, J. Tanaka, *Langmuir* **2011**, *27*, 7645.
[31] M. Tagaya, T. Ikoma, T. Takemura, N. Hanagata, M. Okuda, T. Yoshioka, J. Tanaka, *Langmuir* **2011**, *27*, 7635.
[32] M. Tagaya, T. Ikoma, N. Hanagata, T. Yoshioka, J. Tanaka, *Sci. Technol. Adv. Mater.* **2011**, *12*, 034411.
[33] N. Li, A. Tourovskaia, A. Folch, *Crit. Rev. Biomed. Eng.* **2003**, *31*, 423.
[34] H. Lorenz, M. Despont, N. Fahrni, J. Brugger, P. Vettiger, P. Renaud, *Sens. Act. A* **1998**, *64*, 33.
[35] G. Sauerbrey, *Z. Phys.* **1959**, *155*, 206.
[36] M. Tagaya, T. Yamazaki, S. Migita, N. Hanagata, T. Ikoma, *Bioceram. Develop. Appl.* **2010**, *1*, D110157.

[37] M. Tagaya, T. Ikoma, T. Takemura, S. Migita, M. Okuda, T. Yoshioka, N. Hanagata, J. Tanaka, *Bioceram. Develop. Appl.* **2010**, *1*, D110165.
[38] M. Joshi, R. Pinto, V. R. Rao, S. Mukherji, *Appl. Surf. Sci.* **2007**, *253*, 3127.
[39] W. (V.) S. Gutowski, D. Y. Wu, S. Li, *J. Adhesion* **1993**, *43*, 139.
[40] R. Foerch, J. Izawa, J. Spears, *J. Adhesion Sci. Technol.* **1991**, *5*, 549.
[41] T. Ye, E. A. McArthur, E. Borguet, *J. Phys. Chem. B* **2005**, *109*, 9927.
[42] M. Jonsson, H. O. Johansson, *Colloids Surf. B: Biointerf.* **2004**, *37*, 71.